Freezing conditions in warm disks: snowlines and their effect on the chemical structure of planet-forming disks

Leemker, M.

Chapter 1

Introduction

Earth is the only inhabited planet that we know of to date. Over 5000 exoplanets have been discovered but whether any of them have life on them is unknown. Some exoplanets are extremely hot and life as we know it is impossible, but others are located just far enough from their host star to potentially have liquid water on their surface, a key ingredient for habitability. To understand if the Earth is truly unique in its ability to host complex life, we need to understand the process of star and planet formation and the changes in the chemistry during this process. Comparing the Earth and our Solar System to exoplanets and young, forming planets opens a window to look across the timeline of planet formation. This thesis focuses on the temperature and chemistry of the environment in which young planets are forming.

1.1 Star and planet formation

The cycle of star and planet formation starts with a molecular cloud, see the first panel of Fig. 1.1. As the name suggests, these clouds mainly consist of gas-phase molecular hydrogen (H_2) with trace amounts of CO (Frerking et al. 1982; Lacy et al. 1994). The very low temperatures of $10-20$ K prevent molecules beyond H_2, N_2, and some CO to be in the gas phase at high abundances (Bergin et al. 2002; Caselli et al. 2002), though some clouds like TMC-1 are rich in long carbon chains and aromatic molecules at low abundances (e.g., McGuire et al. 2018; Cernicharo et al. 2023, and references therein). Typical gas-phase densities in these clouds range from $10^4 - 10^6$ particles per cm^3 (see Bergin & Tafalla 2007, for a review) and only 1 % of the mass of a cloud consists of (sub)micron sized dust particles (Draine 2003). Despite their low mass compared to the total gas mass, these dust particles are key to form water and complex organic molecules, the building blocks of life, see Section 1.3.2.

Molecular clouds range from relatively small, irregularly shaped ones of $\sim$ 0.05 pc in size to filamentary giant clouds of 100 pc in diameter (Bok & Reilly

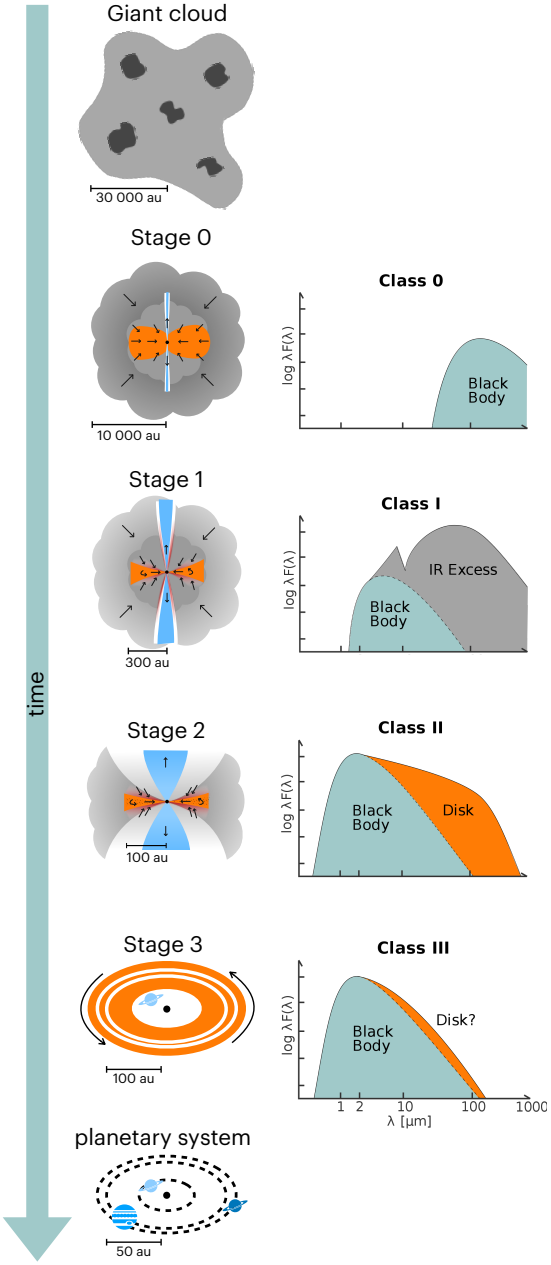

Figure 1.1: Cycle of star and planet formation. Left: theoretical stages from cloud to planetary system. Right: typical SEDs corresponding the the Stages. Figure adapted from M. Persson.

1947; Lada & Lada 2003; Krumholz et al. 2014; André et al. 2010; Hacar et al. 2013, 2017). As the cloud evolves, these cloud cores become denser and colder to the point where their internal gas pressure, turbulent motions, and magnetic field cannot support the cloud cores from gravitational collapse. The mass at which a core becomes unstable is the Jeans mass and may be triggered by the slow evolution of the cloud or due to external factors (Jeans 1928). The cloud core then collapses from the inside out to form a protostellar core of $\sim 10^4$ au (second panel in Fig. 1.1) that then contracts to form one or multiple young protostars surrounded by a massive envelope (Shu 1977; Terebey et al. 1984; Galli & Shu 1993).

The subsequent evolution from the moment a protostar forms to the moment a debris disk is present around the star is characterized by four stages (Shu et al. 1987; Robitaille et al. 2006) that correspond to the same number of observational classes (Lada 1987; André et al. 1993). These classes are defined based on the bolometric temperature and luminosity, the sub-mm luminosity, and the slope of the spectral energy distribution in between 2 and 20 μm ($\alpha_{\rm IR}$ Lada 1987; André et al. 1993; Greene et al. 1994). Even though the different stages show a close correspondence to the classes, the geometry of the source, e.g. an edge-on disk, may cause a misclassification of these objects (Crapsi et al. 2008).

The first stage, Stage 0 is characterized by a protostar surrounded by a massive, several 1000 au envelope, with a mass much larger than that of the star. As the initial core always has some small net angular momentum and because angular momentum is conserved, the gas and dust in the cloud cannot fall onto the star following a straight line. Instead, the material falls to the plane perpendicular to the rotation axis and then spirals inwards forming a pseudo-disk (Cassen & Moosman 1981; Terebey et al. 1984; Galli & Shu 1993). Material from this pseudo-disk is then accreted onto the star at a high rate of $\dot{M}_\star > 10^{-6}$ M$_\odot$ yr^{-1}. The angular momentum that is not stored in the disk or the envelope is removed by a collimated jet that emerges from the envelope. Observationally, these objects are classified through their low bolometric temperature of < 70 K, their bright sub-mm emission ($L_{\rm sub-mm}/L_{\rm bol} > 0.5$ %), and the lack of IR emission observed with telescopes before the advent of the JWST.

After $\sim 10^5$ yr, the star has accreted sufficient mass to outweigh its natal envelope and thus enters Stage 1 of star and planet formation, see the third panel in Fig. 1.1 (Kristensen & Dunham 2018). During this stage, the outflow becomes less collimated and the accretion disk surrounding the central star spreads due to the conservation of angular momentum, while the mass accretion rate onto the star remains high at $\dot{M}_\star > 10^{-6}$ M$_\odot$ yr^{-1} up to ~ 0.5 Myr after the onset of star formation. Observations show that these Class I objects are characterized by a positive slope in the IR $\alpha_{\rm IR} > 0$, a warmer bolometric temperature of $70 - 650$ K, and a relatively low sub-mm luminosity compared to the bolometric luminosity.

Once the envelope has dissipated through accretion onto the disk and outflow of material, a pre-main sequence star surrounded by a ~ 100 au protoplanetary disk emerges (Stage 2, see the fourth panel in Fig. 1.1). During this phase, accretion onto the central star has slowed down to a rate $\dot{M}_\star < 10^{-6}$ M$_\odot$ yr^{-1} (Manara et al. 2023, for a review). As planet formation likely starts in the Class 0 or Class I phase,

protoplanetary disks are also referred to as planet-forming disks (e.g., Segura-Cox et al. 2020; Tychoniec et al. 2020). Within the following $5 - 10$ Myr, the planets continue to accrete disk material and the remaining gas and dust is cleared from the system through MHD disk winds and photoevaporation. As the emission from the central star is not attenuated as much by the surrounding envelope, these objects have an intermediate spectral index of $-1.5 < \alpha_{\rm IR} < 0$ and a high bolometric temperature of $650 - 2800$ K and are classified as Class II objects.

The third and final stage before a planetary system emerges is the debris disk stage (see the fifth panel in Fig. 1.1). In contrast to the gas-rich Stage 2 disk, the debris disks are gas-poor and the dust is likely of secondary origin due to collisions of planetesimals. The gas in many debris disks is consistent with a secondary origin though some may contain primordial gas from the protoplanetary disk phase (Kral et al. 2017; Hughes et al. 2018). Their spectral energy distribution only shows a small amount of excess emission in the (sub)-mm regime with a spectral index $\alpha_{\rm IR} < -1.5$. After the disk has vanished, the star reaches the main sequence and is surrounded by a planetary system of exoplanets.

1.2 Protoplanetary disks

1.2.1 Evolution of disks

The direct detection of two young planets in the PDS 70 disk shows that planet formation is ongoing in disks. Disk formation is a natural outcome of the star formation process as disks are seen around many young stars (e.g., Ansdell et al. 2016; Manara et al. 2023). Both simulations and observations show that protoplanetary disks can form as early as in the Class 0 stage (Yorke et al. 1993; Tobin et al. 2012; Murillo et al. 2013). As the disk evolves its mass increases because the accretion rate of envelope material onto the disk is higher than the accretion rate of disk material onto the star (Hueso & Guillot 2005). Therefore, the disk mass increases over time till the system reaches a high disk-to-star mass ratio, possibly leading to a globally gravitationally unstable disk (Kratter & Lodato 2016; Xu & Kunz 2021a,b). Gravitational instability (GI) leads to spiral arms and clumps of material that can collapse to form a binary stellar companion or a young planet.

Another effect of a disk instability or an external trigger such as a flyby of a nearby star is the triggering of a protostellar outburst (see Kenyon & Hartmann 1987; Fischer et al. 2023, for a review). During an FU Orionis type outburst, the luminosity of the star increases by orders of magnitude and slowly decreases over a timescale of tens to over 100 yr before the luminosity approaches that before the outburst began. Additionally, stars accrete $10^{-3} - 10^{-2}$ $M_\odot$ of material during this brief period due to the very high accretion rates that are observed (Audard et al. 2014).

As the disk further evolves the ratio of disk mass to stellar mass decreases to $10^{-1} - 10^{-4}$ due to accretion onto the central star, disk winds, and potentially by locking up material in newly formed planets (Manara et al. 2023). Even though the mass budget of a young star-disk system is dominated by the central star, the angular momentum is largely contained in the rotating disk. A consequence of the

conservation of angular momentum is that protoplanetary disk material cannot accrete onto the central star unless the angular momentum is redistributed across the disk.

The redistribution of angular momentum drives the evolution of the disk in time. Two leading hypotheses for the mechanism behind this are viscous evolution (Lynden-Bell & Pringle 1974; Pringle 1981) and magneto-hydrodynamic (MHD) disk winds (e.g., Lesur et al. 2013; Bai 2016). Both processes can be active at the same time in the disk but viscous evolution likely dominates the earlier phases while MHD driven disk winds dominate the later phases (e.g., Trapman et al. 2022).

The rotation velocity in a Keplerian disk is not constant but decreases with the square root of the distance from the star. Therefore, two adjacent annuli of gas experience a shearing force between them with the inner ring being slowed down and the outer one being sped up due to their velocity difference. This process transfers part of the angular momentum of the inner ring to the outer ring at an efficiency set by the disk viscosity (Shakura & Sunyaev 1973; Lynden-Bell & Pringle 1974; Pringle 1981; Hartmann et al. 1998). The driver of this viscosity is unknown but numerous processes have been suggested such as GI, vertical shear instability, and magneto-rotational instability, whereas the Brownian motion of gas-phase molecules is too low and thus excluded as the main driver of the viscosity (Lin & Pringle 1987; Balbus & Hawley 1991; Richard & Zahn 1999; Nelson et al. 2013; Stoll & Kley 2014; Armitage 2019). Recent observations of disks show that turbulence and thus the viscosity is low in most disks (e.g., Flaherty et al. 2015, 2017, 2018; Teague et al. 2018b; Trapman et al. 2020). Regardless of the source of the disk viscosity, the inner disk loses the angular momentum that the outer disk gains causing the material in the inner disk to accrete onto the star while the outer disk spreads outwards. The viscous spreading of the disk is one of the main observational discriminators between the viscous evolution model and the disk wind model.

MHD disk winds on the other hand, redistribute angular momentum by removing material from the disk surface layers along the magnetic field lines if the gas is sufficiently ionized to couple to the magnetic field (see Pascucci et al. 2023, for a review). Along with the removal of a small amount of gas mass, a large amount of angular momentum is removed. Detailed modelling of these disk winds shows that the removal of angular momentum is sufficient to drive accretion onto the central star (Ferreira et al. 2006; Béthune et al. 2017; Zhu & Stone 2018; Tabone et al. 2022a,b). In contrast to viscous evolution, MHD driven evolution predicts that the disk radius shrinks over time. Even though only a few spatially resolved disk winds or disk wind candidates have been observed with ALMA in Class II disks (Louvet et al. 2018; Booth et al. 2021a; Pascucci et al. 2023), distinguishing viscous evolution from MHD disk winds as the main driver of disk evolution remains an active topic in the field (Manara et al. 2023).

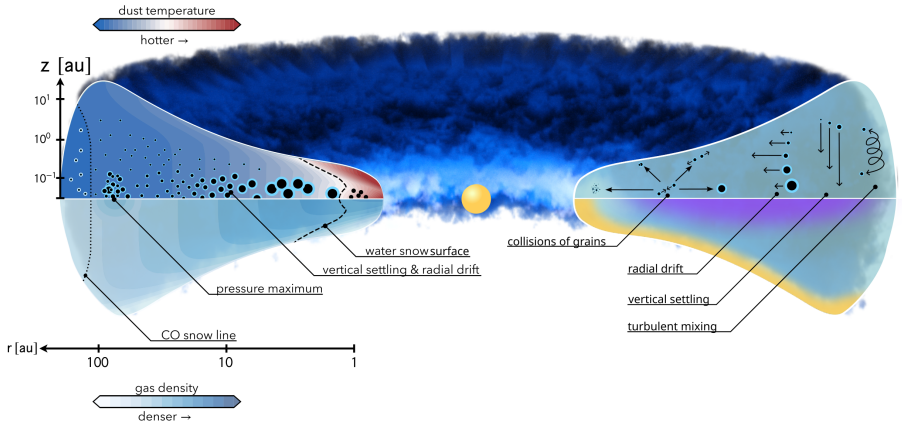

Figure 1.2: Schematic view of a protoplanetary disk. Left: temperature and density structure. Right: four main processes involving dust grains in a disk. Collisions between grains can result in four possible outcomes (counterclockwise): sticking, bouncing, mass transfer with some fragmentation, fragmentation. Figure adapted from Testi et al. (2014) and Miotello et al. (2023).

1.2.2 Dust evolution and planet formation

Another big question in the field is the formation of planets. Protoplanetary disks disperse on a timescale of a few million years (e.g., Haisch et al. 2001; Fedele et al. 2010), so planet formation must happen fast. The formation of planets starts with the micron-sized dust particles that a protoplanetary disk inherits from the molecular cloud. Frequent collisions between these dust particles and gas-phase molecules force the dust to follow the gas. Therefore, these small grains are seen in all disk layers, see Fig. 1.2. In addition to collisions with gas-phase molecules, the dust particles also collide with each other to form larger grains up to a few mm in size due to efficient sticking (e.g., Blum & Wurm 2008; Brauer et al. 2008; Wada et al. 2008; Birnstiel et al. 2010; Güttler et al. 2010; Birnstiel et al. 2012). Observations of Class 0 and I objects already show evidence for grain growth (Kwon et al. 2009; Harsono et al. 2018; Tychoniec et al. 2020).

During this process the larger dust grains decouple from the gas due to their increase in size and thus Stokes number. This causes these particles to settle towards the disk midplane due to a net gravitational force in this direction (see Fig. 1.2, Dubrulle et al. 1995; Villenave et al. 2020). In addition, the decoupling from the gas increases the relative velocities between the dust particles causing the particles to bounce or fragment instead of growing. As the fragmentation velocity of these particles is low at $1 - 10$ m s^{-1}, dust growth beyond the fragmentation barrier seems impossible without invoking additional mechanisms to increase sticking or reduce fragmentation.

Even if cm-sized pebbles continue growing to boulders of $\sim$ 1 m, retaining them in the disk to form planets is unlikely without anything to stop radial drift. The reason for this is that the gas rotates at a slightly sub-Keplerian velocity due to the gas pressure. The decoupled pebbles and boulders do not feel this gas pressure and thus rotate at the Keplerian velocity appropriate for their distance from the central star. The boulders thus feel a head wind from the gas in the disk, transferring their angular momentum to the gas and causing the boulders to drift towards the central star on a timescale of only 100 yr at a distance of 1 au from the star (Whipple 1972; Weidenschilling 1977). For mm size dust grains, the timescale is $\sim$ 1 Myr at a distance of 100 au in the outer disk, respectively. An example of this process in a protoplanetary disk is provided by the CX Tau disk where the dust has drifted inwards to a radius five times smaller than that of the gas disk (Facchini et al. 2019).

Radial drift can be slowed down or even stopped in the pressure traps in a disk. A maximum in the gas pressure causes the particles to drift towards this location instead of drifting to the inner regions of the disk (e.g., Pinilla et al. 2012b,a). Many different mechanisms have been proposed to create these traps such as the outer edge of a gap carved by a massive planet, but also processes that do not require a planet to be present like GI, zonal flows, vortices, magneto-rotational instability, and the inner edge of dead zones (a disk region with low ionization suppressing the magneto-rotational instability; see Pinilla et al. 2017; Bae et al. 2023, for reviews). These pressure bumps provide a favourable location to grow pebbles and boulders into km-sized planetesimals due to the slower radial drift and smaller velocity differences between bodies reducing the chance of fragmentation upon a collision. GI not only creates spiral arms that act as pressure traps; the collapse of disk material can also directly form planets or stellar companions in the outer disk that could create new pressure traps (Boss 1997; Boley 2009; Kratter et al. 2010).

In addition, snowlines, i.e., the midplane radii where one of the major volatiles in the disk freezes-out onto the dust grains, may be a location where planet formation is enhanced. Especially the water snowline may be a good candidate as water is the first major volatile to freeze out. The diffusion of water across the snowline feeds the ice and thus increases the mass of solids just outside the water snowline (Stevenson & Lunine 1988). This not only provides additional mass to form planets, it could also trigger the streaming instability causing the dust particles to further concentrate and possible collapse to form larger bodies (Youdin & Goodman 2005; Johansen et al. 2007; Drążkowska & Alibert 2017; Schoonenberg & Ormel 2017). The dust grains outside the water snowline may be somewhat more prone to fragmentation due to their icy mantles, these mantles also increase the probability of two colliding grains to stick together and thus grow (Wada et al. 2011; Okuzumi et al. 2016).

Once planetesimals have formed, two main pathways to form planets are hypothesised: planetesimal accretion and pebble accretion (see Drążkowska et al. 2023, for a recent review). Both mechanisms have in common that they are driven by gravity, but their differences arise from the sizes of the initial bodies (planetesimals vs pebbles). In the case of planetesimal accretion, the formation of planets is

driven by collisions of planetesimals where the largest bodies have the largest gravitational pull and thus the highest accretion rates (Kokubo & Ida 1996; Tanaka & Ida 1999). However, this process can also lead to fragmentation and it is too slow to form a sufficiently massive solid core ($\gtrsim$ 10 M_{Earth}) to accrete gas and form a giant planet at the distance of the ice giants in our Solar System (Pollack et al. 1996; Ikoma et al. 2000; Thommes et al. 2003). Pebble accretion provides a solution to this timescale problem as the accretion of pebbles onto a solid core is orders of magnitude faster than planetesimal accretion (Ormel & Klahr 2010; Lambrechts & Johansen 2012; Johansen & Lambrechts 2017). However, pebble accretion is only efficient if sufficiently massive cores to accrete onto are already present in the disk.

Comparing the exoplanet population that is observed to date to the planet forming disks could hold important clues to understand the planet formation process. One of these clues may be the disk mass as observations of protoplanetary disks in the Class II phase show that their masses are generally too low to explain the masses of the exoplanets around main sequence stars (e.g., Ansdell et al. 2016; Manara et al. 2018). The younger Class 0 and I disks are more massive and could reproduce the observed exoplanet population (e.g., Tychoniec et al. 2018, 2020; Tobin et al. 2020). However, these masses may be an underestimate of the true disk mass as the continuum emission is likely optically thick, hiding part of the dust mass, dust may have grown to larger sizes than those probed by the observations, and the dust opacity may be underestimated due to scattering (Zhu et al. 2019). Even though observations suggest that planet formation may start early, this does not mean that planet formation is finished before the Class II phase is reached.

1.2.3 Observations of disks with ALMA

Protoplanetary disks are observed with many different telescopes such as the VLT, NOEMA, SMA, VLA, ALMA, and recently JWST. ALMA is of particular interest for this thesis as its observing frequency, spatial and spectral resolution, and sensitivity are particularly well suited to spatially resolve the dust structures due to pressure traps and the weak molecular line emission probing the gas.

ALMA is a radio interferometer located on a plateau 5000 m above sea level in the Chilean desert. The 66 telescopes of ALMA are divided into three groups: the main array consisting of 50 antennas with a diameter of 12 m, the ACA consisting of 12 antennas of 7 m, and the Total Power array consisting of four 12 m antennas. As each group probes a larger angular scale on the sky, the main array, sometimes in combination with the ACA are most frequently used for protoplanetary disk observations.

The spatial resolution of the main array is tuned to the specific needs of observations as every $\sim$ 20 days the telescopes of the main array are moved to a new configuration and thus a different spatial resolution. The highest resolution of $0\farcs01$ at 870 GHz or $0\farcs04$ at 230 GHz is achieved in the most extended configuration (C-8), whereas the lowest resolution of $3\farcs4$ at 100 GHz or $1\farcs5$ at 230 GHz is obtained in the most compact configuration (C-1). The maximum scale that

can be probed by these configurations is an order of magnitude larger than the respective spatial resolution as interferometers are not sensitive to extended emission. Therefore, multiple configurations are combined if a high dynamic range in spatial scales is expected.

ALMA covers a wide frequency range of $84 - 950$ GHz divided into eight (non-continuous) frequency bands, Band $3 - 10$. In addition, ALMA Band 1 ($35 - 50$ GHz) is currently being installed and expected to be offered from March 2024 and ALMA Band 2 ($67 - 116$ GHz) is in development. The wide range in available frequencies can not only be used for multi wavelength observations of the continuum to constrain e.g., the grain sizes and continuum optical depths but also to probe molecular lines with different upper energy levels. In particular, the high frequency bands, Band $8 - 10$ can be used to probe warm molecular lines, such as the ^{13}CO $J = 6 - 5$ transition that cannot be observed otherwise (see also Chapter 4). The wide frequency range together with the high spatial and spectral resolution and sensitivity of ALMA enable both detailed studies of individual disks (e.g., Qi et al. 2013; Cleeves et al. 2015b; Isella et al. 2016; Schwarz et al. 2016; Pinte et al. 2018b; Teague et al. 2018a,b; Wölfer et al. 2021; Keyte et al. 2023; Law et al. 2023a) and surveys of larger samples (Andrews et al. 2013; Miotello et al. 2014; Ansdell et al. 2016; Barenfeld et al. 2016; Miotello et al. 2016; Tripathi et al. 2017; Andrews et al. 2018; Ansdell et al. 2018; Long et al. 2018; Öberg & Bergin 2021; Anderson et al. 2022; van Terwisga et al. 2022; Stapper et al. 2022; Wölfer et al. 2023b).

1.2.4 Disks are not smooth in dust

The most striking direct proof of ongoing planet formation in a protoplanetary disk is the detection of two young, accreting planets in the PDS 70 disk (Keppler et al. 2018; Haffert et al. 2019; Benisty et al. 2021). These young planets are sufficiently massive to carve a wide gap and thus create a pressure trap just outside of their locations in the PDS 70 disk. Many of the structures seen in other protoplanetary disks to date can also be explained by embedded massive planets as rings and gaps are seen at almost all radii in large and bright disks observed with ALMA (see Fig. 1.3; e.g., Andrews et al. 2018; Long et al. 2018; Huang et al. 2018). However, even though the majority of structures can potentially be explained by planets, individual rings and gaps can be due a dust opacity change around the water snowline, a dead zone, and other processes forming pressure traps in disks (e.g., Huang et al. 2018).

In addition to rings and gaps, some disks show spiral arms in the sub-mm continuum (see e.g. IM Lup and Elias 27 in Fig. 1.3). Spiral arms are less common in the sub-mm emission than rings and gaps, and are likely generated by forming planets, binary companions, zonal flows, or a gravitationally unstable disk (e.g., Ogilvie & Lubow 2002; Rafikov 2002; Dong et al. 2015a; Uribe et al. 2015; Kratter & Lodato 2016; Bae & Zhu 2018). Another azimuthal structure that is sometimes seen in disks is an arc (see e.g., HD 143006 and HD 163296 in Fig. 1.3 and IRS 48 continuum in the top left panel of Fig. 1.5). These arcs can be the result of vortices due to a massive planer or stellar companion triggering the Rossby-Wave

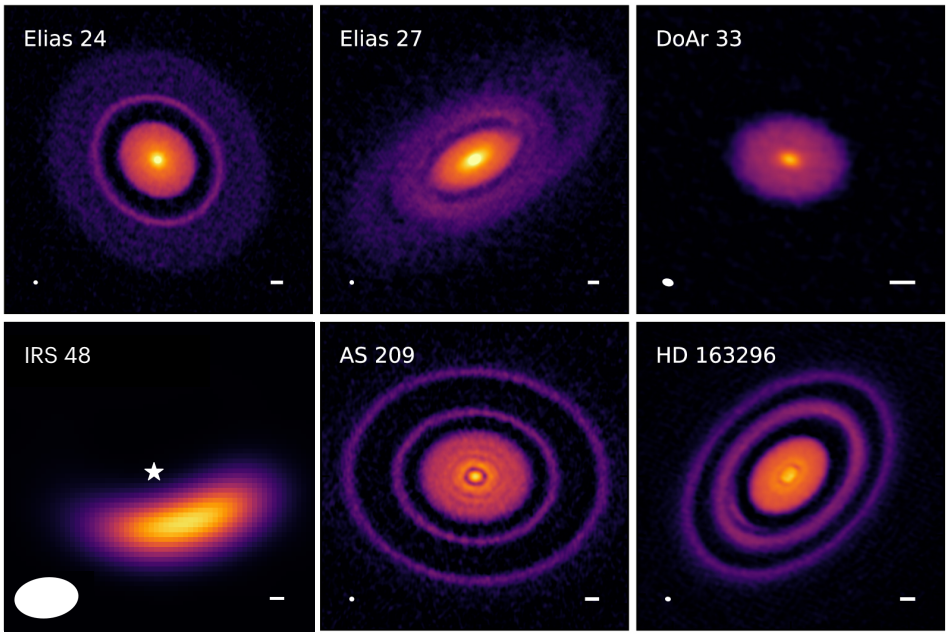

Figure 1.3: Continuum observations of structured protoplanetary disks. Rings, gaps, spirals, and an arc are seen. The resolution of the observations is indicated with the white ellipse in the bottom left corner and a 10 au scale bar is indicated in the bottom right corner. Figure adapted from van der Marel et al. (2013) and Andrews et al. (2018).

instability (Lovelace et al. 1999; Li et al. 2000, 2001; van der Marel et al. 2013).

Observing these rings, gaps, spirals, and arcs is now common with ALMA due to its high spatial resolution. However, even before the advent of ALMA disks with large cavities, transition disks, were identified based on their SED at IR to (sub-)mm wavelengths. The SED of transition disks is characterized by a low MIR and in some cases also NIR fluxes tracing the lack of the warm dust close to the central star. Excess emission at NIR wavelengths is indicative of a small dusty inner disk close to the central star. Gas observations with ALMA show that these disks not only have a deep cavity in the dust, but often also in the gas (e.g., Bruderer et al. 2014; Perez et al. 2015; van der Marel et al. 2015, 2016; Wölfer et al. 2021, see also Chapter 4). These cavities are likely due to one or more massive planets or a stellar companion but also photoevaporation can clear the inner disk regions from gas and dust (Owen et al. 2011; Ercolano & Pascucci 2017; Picogna et al. 2019). Interestingly, despite their large cavities, the observed accretion rates of these disk are often high, much higher than expected based on the mass of the dusty inner disk if present, suggesting that gas must flow through the cavity at high velocities (e.g., Najita et al. 2007; Espaillat et al. 2014; Francis & van der Marel 2020; Manara et al. 2020).

1.2.5 Disks are not smooth in gas

The dust in protoplanetary disks only makes up 1% of the total disk mass. Therefore, observations of the gas are needed to fully understand planet formation. Despite the fact that 99% of the disk mass consists of gas, observations of it are much more difficult than continuum observations. The reason for this is that a gas-phase molecule only emits at certain narrow frequency ranges (emission lines) set by quantum mechanics in contrast to the dust that emits at all wavelengths similar to or smaller than the grain itself (Draine 2006). Additionally, the flux of a specific gas line that is observed is set by the number molecules and the gas temperature. To further complicate gas observations, the most abundant molecule in a disk, molecular hydrogen, does not have a permanent dipole moment and thus no strong rotational transitions tracing the bulk of the disk. Therefore, less abundant molecules with a permanent dipole moment are used to trace the gas in disks.

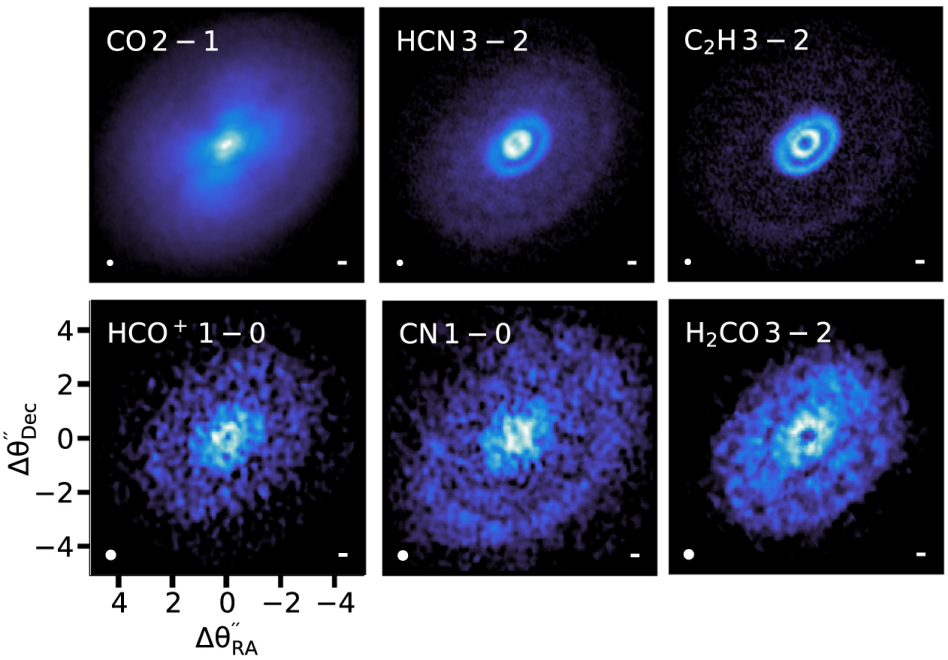

Figure 1.4: Diversity of structures in the HD 163296 disk. Figure adapted from Öberg & Bergin (2021).

One of the most commonly used tracers of the gas in a disk are CO and its isotopologues. CO is the second most abundant molecule with a typical abundance of only 10^{-4} with respect to hydrogen, yet CO rotational lines are often optically thick. As CO is abundant in almost all disk regions, CO and its isotopologues have often been used to estimate the radial extent of the disk as well as the mass.

In addition to CO and its isotopologues, over 40 other molecules and isotopologues have been detected in disks to date (McGuire 2022). A gallery of a few

different molecules in the HD 163296 disk is shown in Fig. 1.4. Similar to the diversity in dust substructures, these gas-phase molecules also all show rings and gaps at different radii that do not correlate with the dust in general (Law et al. 2021a; Jiang et al. 2022). Instead, their emission profiles are set by a combination of temperature and abundance that is controlled by chemical reactions in the disk, which opens the possibility to probe many different processes in the disk as is discussed in Sect. 1.3. However, not all disks conform to this general trend, such as the HD 100546 disk where molecular emission coincides with the dust rings as analysed in this thesis (Chapter 5 and 6).

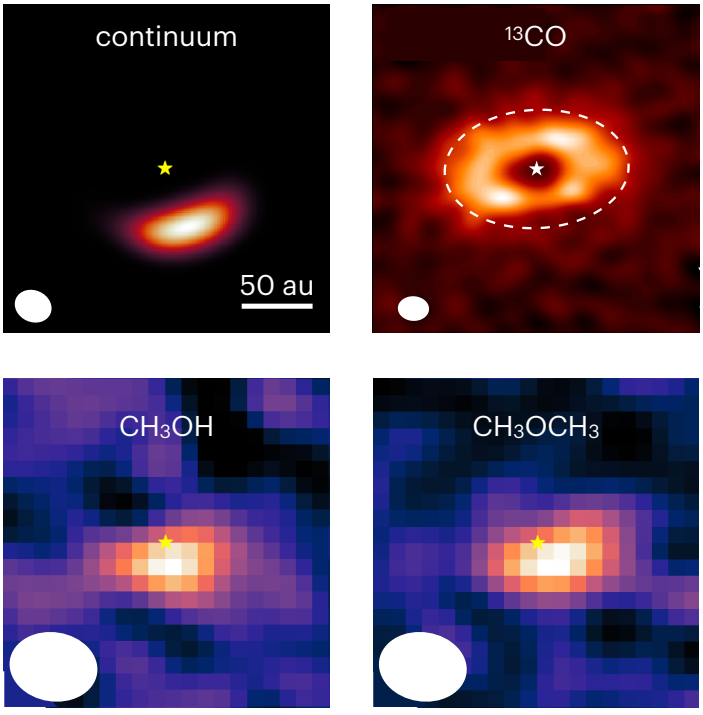

Figure 1.5: The major asymmetric ice trap IRS 48. The large dust (top left panel) is concentrated in the south, whereas the ^{13}CO gas disk is consistent with an azimuthally symmetric disk (top right panel). Emission from COMs (bottom row) is only seen at the dust trap, indicating an origin in the ice. Figure adapted from van der Marel et al. (2016) and (Brunken et al. 2022).

1.2.6 Dust traps are ice traps

Despite the general trend that gas and dust structures do not correlate, two disks are a notable exception: IRS 48 and HD 142527. Both of these disks are transition disks with an asymmetric dust trap but a gas disk that is consistent with an azimuthally symmetric disk (Casassus et al. 2013; van der Marel et al. 2013; Bruderer et al. 2014; van der Marel et al. 2021a). However, the molecular abundances

in these disks (anti-)correlate with the dust instead of the gas. In the IRS 48 disk, emission of H_2CO and COMs is only seen at the location of the dust trap, see Fig. 1.5 (van der Marel et al. 2021b; Booth et al. 2021b; Brunken et al. 2022), whereas in the HD 142527 disk, the emission of CS and H_2CO is seen opposite to the dust trap likely due to a misaligned inner disk shadowing parts of the outer disk (Temmink et al. 2023).

The emission of H_2CO together with multiple COMs at the dust trap in the IRS 48 disk suggests that the gas and dust interact through the thermal sublimation of ices on large dust grains and subsequent vertical mixing if the dust trap is sufficiently warm. The lack of COM emission in the HD 142527 dust trap is consistent with its much lower temperature due to the larger distance to its host star. The temperature of the dust trap can also have a significant impact on the ices that are transported to the inner disk and thus on the molecules and atoms available for forming planets inside the dust trap (e.g., van der Marel et al. 2021c).

1.2.7 Vertical structure in disks

The cartoon of a protoplanetary disk in Fig. 1.6 shows that disks do not only have a steep gradient in their density, temperature, and UV field in the radial direction but also in the vertical direction. The surface layers of the disk are directly exposed to the UV field of the central star, increasing their temperature. The intense UV field not only heats the disk, it also photodissociates many of the molecules present in this layer. Additionally, the X-rays impinging on this layer ionize the remaining atoms and molecules. In contrast, the cold and dense disk midplane is dominated by gas containing only the most volatile molecules such as H_2 and CO, and dust grains covered in icy layers.

At intermediate disk layers, the UV and X-ray fields are (partially) shielded allowing molecules to survive and react with each other. Therefore, this layer is characterized by a rich chemistry and will be further explored in Sect. 1.3. ALMA observations at high spatial and spectral resolution and sensitivity can directly measure the radial and vertical location at which a molecular line emits in a disk (e.g., Pinte et al. 2018a; Paneque-Carreño et al. 2022, 2023; Law et al. 2021b). This can not only be used to probe the emitting layer of different molecules or different lines of the same molecule, it can also be used to probe the 2D temperature structure in disks using multiple optically thick isotopologues of CO that probe deeper and deeper into the disk.

1.3 Astrochemistry

The composition of the gas and ice in protoplanetary disks and other objects is set by the chemical reactions between atoms and molecules. These chemical reactions are operating under very different conditions than those on Earth as typical densities in protoplanetary disks correspond to those in the highest vacuum that can be created in state of the art laboratories on Earth. Therefore, collisions between molecules are rare and the chemical timescales are long. Still a rich

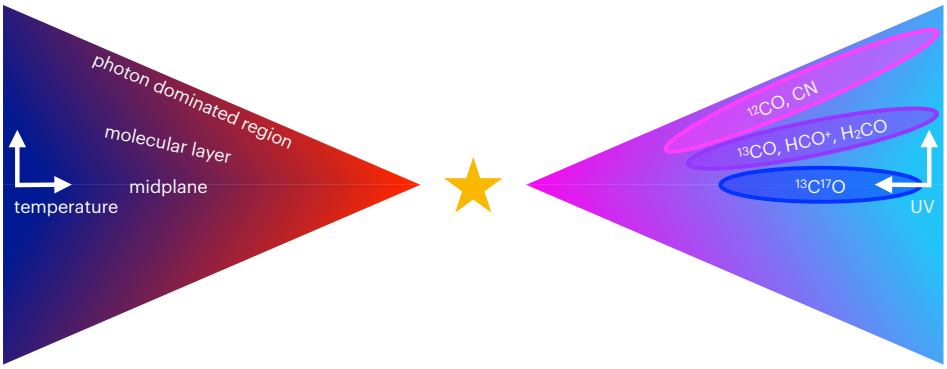

Figure 1.6: Schematic view of the radial and vertical structures in a protoplanetary disk. Left: temperature structure. Right: layering of molecules.

molecular complexity is seen across all stages of star and planet formation (e.g., Herbst & van Dishoeck 2009; Caselli & Ceccarelli 2012). The molecules that are detected vary from very simple molecules such as H_2 up to H_2O and the building blocks of life and other complex organic molecules (COMs, molecules that consist of at least six atoms of which at least one carbon and one hydrogen atom; see McGuire 2022 and references therein).

Understanding this rich molecular inventory not only requires observations of these molecules, but also laboratory research and quantum calculations to quantify the reaction rates, branching ratios, and reactions products. These reactions are collected in large databases to make predictions for the abundances of molecules in clouds and protoplanetary disks (e.g., UMIST and KIDA; Wakelam et al. 2012; McElroy et al. 2013). The reactions in most chemical networks are divided into two categories: gas-phase reactions and grain-surface reactions (see e.g., Tielens 2003; van Dishoeck 2014, for reviews).

1.3.1 Gas-phase chemistry

Two of the molecules that form predominantly through gas-phase reactions are CO and HCO^+, but also other molecules like C_2H and O_2 are formed in the gas. The gas-phase reactions are dominated by two body reactions as the probability of three or more atoms or molecules meeting simultaneously is negligibly small due to the low gas density. Additionally, ions and molecules with a permanent dipole moment are more likely to react with other molecules due to their long range interactions (ion-molecule reactions), whereas the interactions between two neutral molecules are slower.

The low gas temperature in astronomical environments not only makes collisions between molecules rare due to their low velocities, it also heavily favours exothermic reactions over endothermic reactions and reactions with energy barriers as there is hardly any energy available. The additional energy that is produced during exothermic association reactions further limits the reactions that can take

place. This is due to the conservation of energy. If two molecules react to form a single new body, the excess energy from the bond can only be released through the emission of a photon in the gas phase, which is a very slow process. Therefore, the chance of immediate dissociation of the newly formed molecule is high and the efficiency of the initial reaction is thus low. Bond rearrangement on the other hand is much more efficient as not one but two reaction products are formed in a chemical reaction. The lightest of these two carries most of the excess energy as kinetic energy, thus stabilizing the molecule that has formed.

1.3.2 Grain surface chemistry

Reactions on the surfaces of grains are essential to form the most abundant molecule in the universe, H_2 as well as H_2O and COMs. Gas-phase atoms and molecules can land on a grain and freeze out if the temperature is sufficiently low. A light atom such as H is not bound to a specific site on the grain surface, but instead it can scan the surface. If another atom or molecule is encountered during this process this atom or molecule is hydrogenated. For instance, water is formed through $O + H \rightarrow OH$, where the excess energy is absorbed by the grain, allowing the OH radial to survive. When another hydrogen atom reacts with OH, H_2O is formed (Tielens & Hagen 1982; van Dishoeck et al. 2013). Similarly, many of the COMs likely form through the hydrogenation of CO ice (Watanabe & Kouchi 2002; Cuppen et al. 2009; Chuang et al. 2016). The processing of CO ice to CO_2 and other complex molecules in the ices could also be responsible for the very faint CO fluxes that are observed in protoplanetary disks (e.g., Favre et al. 2013; Ansdell et al. 2016; Miotello et al. 2017; Bosman et al. 2018b).

The molecules on the grain surfaces can desorb into the gas phase through excess energy produced during their formation (chemical desorption), an incident UV photon (photodesorption), or due to sublimation if the grain is heated (thermal desorption). Therefore, molecules that formed in the ice may also be observed in the gas-phase. The effect of freeze-out and desorption of the major volatiles on protoplanetary disk chemistry is discussed in detail in the next Section.

1.3.3 Inheritance or reset

As the long journey from clouds to protoplanetary disks and then planets mostly happens at temperatures below the freeze-out temperature of water, the question is raised whether the water seen in disks and comets is inherited from the earliest phases of star and planet formation or if the chemistry is reset along the way (e.g., Visser et al. 2009; Furuya et al. 2013; Cleeves et al. 2014b). In the inheritance scenario, the majority of the water that formed in the molecular cloud stage remains frozen out and unaltered through the four stages of star and planet formation until a planetary system is born (Visser et al. 2009; Drozdovskaya et al. 2016). On the other hand, in the reset scenario, water may still form in the molecular cloud stage, but this water is destroyed and later reformed during at least one of the stages (e.g., Yang et al. 2013). As the conditions under which water is destroyed and subsequently reformed may vary, the water content in e.g. protoplanetary

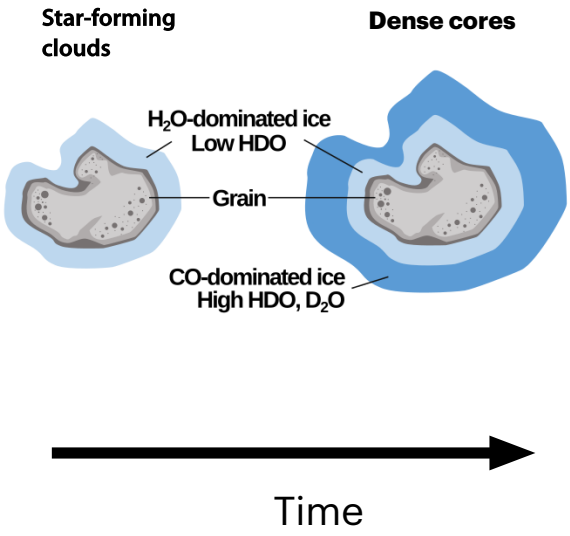

Figure 1.7: Deuteration of ices on a grain. The first layer mainly consists of H_2O ice as deuteration only becomes efficient when the cloud cools down and CO freezes-out creating a second layer dominated by CO ice with high levels of HDO and D_2O. Figure taken from van Dishoeck et al. (2021).

disk is expected to vary between isolated disks and disks in clusters whereas in the inheritance scenario each disk is born with a water abundance of 10^{-4} with respect to hydrogen. Therefore, inheritance vs reset is an important factor that sets the amount of water that is available for forming planets.

As measuring the water content in protoplanetary disks is difficult as discussed in previous sections, a different probe of inheritance vs reset is often used: deuteration of water. In the molecular cloud phase, water forms on the surfaces of grains through grain surface chemistry (see Sect. 1.3.2). Initially, the deuteration levels are low and the ice predominantly consists of H_2O, see Fig. 1.7. As the clouds cool down, the deuteration levels increase due to two main effects. First, the formation of almost all deuterated molecules is driven by H_2D^+ formed through

$$H_3{}^+ + HD \rightarrow H_2D^+ + H_2 + 230 \text{ K}. \tag{1.1}$$

The exothermicity of this reaction limits the backwards reaction at temperatures below $\sim$ 25 K (Watson 1976; Aikawa & Herbst 1999). Second, at temperatures lower than $\sim$ 20 K, the reaction of H_2D^+ with CO is quenched (e.g., Pagani et al. 1992; Roberts et al. 2003). Therefore, deuteration is very efficient in the cold molecular cloud phase (Ceccarelli et al. 2014) and a second layer of ice is formed on the grains. This layer is dominated by CO ice and has high abundances of semi-heavy water (HDO) and heavy water (D_2O), see Fig. 1.7 (Furuya et al. 2016).

As this deuteration process is only efficient in the cold and dense cloud core, a high HDO/H_2O is only expected in the case of inheritance. Observations of HDO

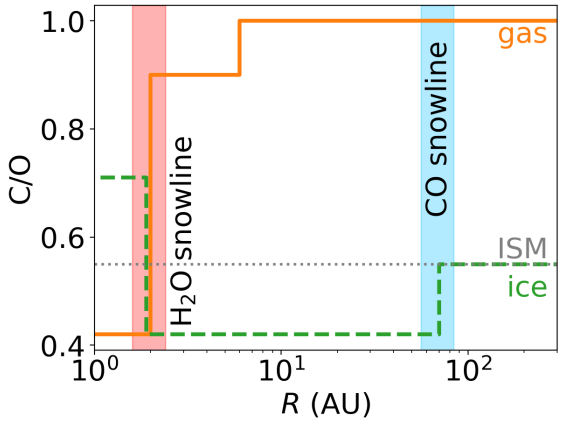

Figure 1.8: Snowlines and their effect on the chemical composition of planet forming material. Figure adapted from Öberg et al. (2011).

and the optically thin $H_2^{18}O$ in Class 0 objects and comets in our Solar system show very similar deuteration levels of $HDO/H_2O \sim 10^{-3}$ (Persson et al. 2014; Altwegg et al. 2015; Jensen et al. 2019, 2021; Altwegg et al. 2019), suggesting that water may be inherited from clouds to comets. However, the destruction of water by UV photons and its subsequent reformation may lead to an HDO/H_2O ratio similar to that in the inheritance case (Furuya et al. 2017). Therefore, the even rarer isotopologue D_2O may be used to distinguish these cases. The first measurement of the HDO/H_2O ratio in a protoplanetary disk is presented in Chapter 3.

1.3.4 Snowlines

The freeze out and thermal desorption of the major volatiles has a large effect on the chemical composition of the planet forming material (e.g., Öberg et al. 2011; Öberg & Bergin 2021). Gas-phase water is one of the first molecules to freeze out as it only desorbs at a high temperature of $\sim 100-150$ K in protoplanetary disks. Therefore, the water snowline in a typical protoplanetary disk is located at only a few au from the host T Tauri star (Harsono et al. 2015). For the warmer Herbig disks, the snowline is expected at a somewhat larger distance of $5-10$ au. Other major snowlines in disks include those of NH_3 and CO_2 that are located a few au outside the water snowline, and the CO and N_2 snowlines that are located at tens of au, see the top bar in Fig. 1.8.

The chemical composition of the planet forming material is often measured as the C/O, C/H, and O/H ratios. The freeze-out of these major volatiles effectively moves carbon and oxygen atoms from the gas-phase into the ice and thus changing these ratios, see Fig. 1.8. In particular the water snowline is important as the largest change in the C/O ratio is seen at that location. In addition, grain growth may be enhanced around the water snowline (see Sect. 1.2.2) making the water snowline a crucial location in the disk. A few au further out, CO_2 freezes out and

the gas-phase C/O ratio approaches unity. A C/O ratio exceeding unity has a dramatic effect on the abundance of C_2H, a molecule that can only be abundant if the C/O ratio exceeds one (e.g., Bergin et al. 2016; Bergner et al. 2019; Miotello et al. 2019; Bosman et al. 2021a; Guzmán et al. 2021). Comparing the chemical composition of the gas and ice in protoplanetary disks to that of exo-planets can provide information on the location where these planets formed.

Directly observing the H_2O and CO snowline in protoplanetary disks is not trivial. First, the location where a molecule freezes-out is a function of both radius and height above the midplane, see Fig. 1.6 in Sect. 1.2.7 for a schematic view. The midplane radius where a 50% of a molecule is frozen out and 50% is in the gas-phase is defined as the water snowline. The water snow surface is the 2D equivalent of this. Therefore, gas phase H_2O and CO can be present out to radii well beyond their midplane snowline locations, hiding the midplane snowline behind a layer of gas in the disk surface. However, the recent detection of H_2O in a protoplanetary disk suggests that the water snow surface may instead be vertical due to vertical mixing causing all water to freeze-out close to the disk midplane (Carr et al. 2018; Bosman & Bergin 2021), the vertical cold finger phenomenon suggested by Meijerink et al. (2009).

Even if the water snow surface is vertical in some disks, locating it is even more challenging than the CO snowline as the water snowline is expected at only a few au from the host star in most protoplanetary disks. The spatial resolution required to resolve the snowline location can only be achieved by ground-based observatories such as ALMA. Even though these observatories are built on high and dry mountains on Earth, the remaining water in the Earth's atmosphere absorbs most of the emission of water in protoplanetary disks and only one detection of gas-phase H_2O with ALMA has been reported to date (Carr et al. 2018; Bosman & Bergin 2021). These telluric lines are avoided by observing the rare isotopologues such as $H_2^{18}O$ or HDO.

1.3.4.1 Tracers of snowlines

As observing these snowlines directly using H_2O or CO is very challenging or impossible, a tracer can be used. A tracer is a molecule that very strongly reacts to the desorption of either H_2O or CO, or a molecule that can only form in the vicinity of the respective snowline. For example, DCO^+ is a molecule that forms efficiently around the CO snowline (Mathews et al. 2013; Carney et al. 2018). Therefore, a ring of DCO^+ is expected around the CO snowline. Observations of the IM Lup disk revealed not one but two CO snowlines in this disk, the inner one due to the thermal structure of the disk and the outer one likely due to non-thermal desorption of CO ice (Öberg et al. 2015). However, DCO^+ also has a warm formation pathway unrelated to the CO snowline, thus careful chemical modelling is required to use it as as snowline tracer (Favre et al. 2015; Qi et al. 2015; Carney et al. 2018).

A molecule that reacts much stronger to the desorption of CO is N_2H^+. This is because CO competes with N_2 to form N_2H^+ and CO also rapidly destroys N_2H^+ (Payzant et al. 1975; Rakshit 1982; Klippenstein et al. 2010). The main

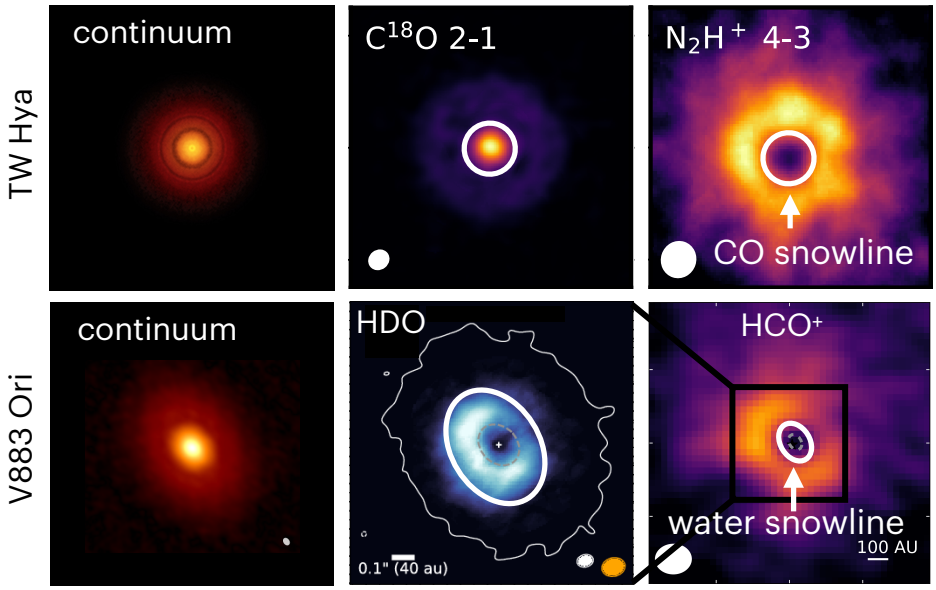

Figure 1.9: Observed anti-correlation between $C^{18}O$ and N_2H^+ tracing the CO snowline (left) and between HDO and HCO^+ tracing the water snowline (right). ALMA observations of the TW Hya disk (left) and the V883 Ori disk (right) taken from (Qi et al. 2013; Andrews et al. 2016; Calahan et al. 2021; Ruíz-Rodríguez et al. 2022; Tobin et al. 2023).

formation pathway of N_2H^+ depends on the disk ionization, it is often used as a tracer of the disk ionization outside the CO snowline (e.g., Aikawa & Herbst 2001; Aikawa et al. 2015; Cleeves et al. 2015b). In addition, gas-phase N_2 is needed to form N_2H^+. Therefore, ring-shaped N_2H^+ emission is expected outside the CO snowline and inside the N_2 snowline, see Fig. 1.9, though detailed chemical modelling is needed to infer these snowline locations (Qi et al. 2013, 2015; van 't Hoff et al. 2017). Observations of N_2H^+ and the rare CO isotopologue $C^{18}O$ and $^{13}C^{18}O$ observationally confirm this anti-correlation (see Fig. 1.9) and thus establish N_2H^+ as a CO snowline tracer (Qi et al. 2013; Zhang et al. 2017). A small survey of N_2H^+ across six disks shows that the snowline locations vary from disk to disk even if a similar temperature is expected based on the spectral type of the host star (Qi et al. 2019).

Two tracers of the water snowline are COMs such as methanol and HCO^+. Methanol has a very similar binding energy to water (e.g., Penteado et al. 2017; Minissale et al. 2022). Therefore, gas-phase methanol is only expected at or inside the water snowline. Following a similar mechanism to N_2H^+ as a CO snowline tracer, HCO^+ traces the water snowline in protoplanetary disks as water efficiently destroys HCO^+, see Fig. 1.9 (Phillips et al. 1992; Bergin et al. 1998; van 't Hoff et al. 2018a) following

$$HCO^+ + H_2O \rightarrow H_3O^+ + CO.$$

This destruction is so efficient that HCO^+ may peak slightly outside the water snowline.

To circumvent the extremely high spatial resolution needed to locate the water snowline in typical T Tauri and Herbig disks, HCO^+ and HDO, an isotopologue of H_2O, are observed in the V883 Ori disk. The central star recently experienced an outburst increasing its luminosity up to ~ 400 $L_\odot$ (Pickering 1890). Over the past century the luminosity has decreased by a factor of ~ 2 (Furlan et al. 2016), but the disk is still significantly warmer than disks around quiesent stars. Observations of the continuum suggested that the water snowline in this disk is located at 40 au based on a sudden change in the continuum opacity (Cieza et al. 2016). However, gas-phase methanol and HDO are seen out to 140 au and ~ 160 au (van 't Hoff et al. 2018a; Tobin et al. 2023). Moreover, ring-shaped HCO^+ emission is seen in this disk with a peak intensity well outside the methanol and HDO emission, see Fig. 1.9. The observed anti-correlation between HCO^+ and methanol are discussed in Chapters 2 and 3.

1.4 Thermometers in disks

The temperature structure of a disk does not only set the snowline locations, it also sets population of the energy levels of molecules and thus the expected line intensity assuming local thermodynamic equilibrium (LTE). Therefore, the temperature structure in a disk cannot only be probed by the abundance of snowline tracers such as HCO^+, N_2H^+, and DCO^+ but also by the intensity of the continuum and molecular line emission. In this section, two additional methods to probe the disk temperature are discussed, one for optically thick line and continuum emission and one for optically thin line emission.

1.4.1 Brightness temperature

The brightness temperature of continuum or molecular line emission is defined as the temperature of a backbody that emits the observed intensity in the Rayleigh-Jeans limit. Therefore, the brightness temperature approximates the temperature of the disk material if the following conditions are satisfied: the emission is optically thick, spatially resolved, spectrally resolved, and the Rayleigh-Jeans approximation is appropriate. In case one of these requirements is not met, the brightness temperature (generally) underestimates the kinetic temperature.

If the emission is optically thin or marginally optically thick and the optical depth is known, the brightness temperature can be corrected for the optical depth τ using $1 - e^{-\tau}$. However, accurate measurements of the optical depth are challenging. Similarly, the brightness temperature can be corrected for unresolved emission if the emitting region is known from e.g., higher spatial resolution observations. As the brightness temperature is directly proportional to the observed intensity it provides an straight forward method to probe the disk temperature of both the dust and of the gas in the emitting layer of molecule.

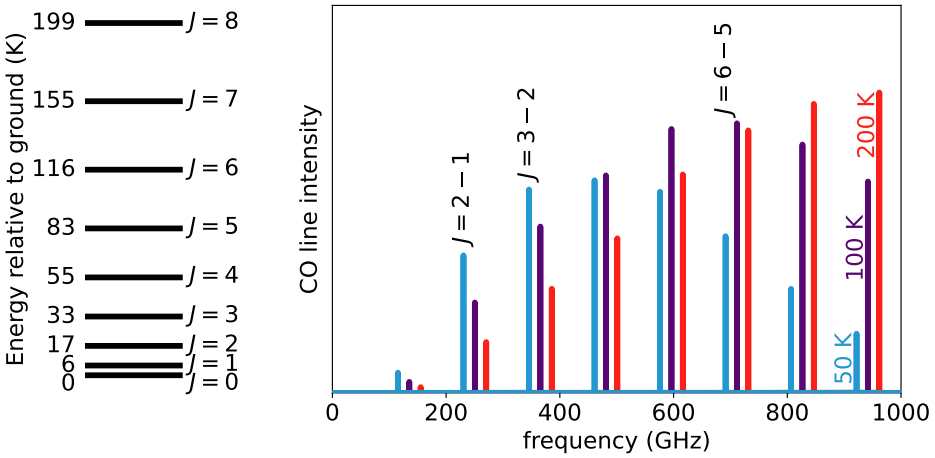

Figure 1.10: Left: CO rotational ladder. Right: the expected line intensities for three different temperatures of 50 K (blue), 100 K (purple), and 200 K (red). The 20 GHz frequency shift is applied to the purple and red spectra for visualisation purposes.

1.4.2 Line ratios

Another method to measure the temperature of the gas is to use line ratios of optically thin transitions (e.g., Goldsmith & Langer 1999; Loomis et al. 2018). The population of the energy levels of a molecule depends on its temperature if the density is sufficiently high:

$$\frac{N_u}{N_{\rm tot}} = \frac{g_u}{Q(T_{\rm ex})} e^{-E_u/(k_B T_{\rm ex})}, \tag{1.2}$$

with N_u the column density of the upper energy level u, $N_{\rm tot}$ the total column density of the molecule, g_u the degeneracy, $Q(T_{ex})$ the partition function at excitation temperature $T_{\rm ex}$, E_u the energy of level u, and k_B the Boltzmann constant. This also affects the expected line intensity as shown in Fig. 1.10.

The column density of the upper energy level can be measured directly from the observations as this is directly proportional to the integrated flux and not dependent on temperature. The right hand side of Eq. 1.2 only depends on molecular properties that can be found in databases such as CDMS and JPL (Pickett et al. 1998; Müller et al. 2001, 2005; Endres et al. 2016) and on the excitation temperature that is equal to the kinetic temperature if the gas is in LTE. Therefore, the gas temperature can be measured directly if two (or more) molecular lines of the same molecule are observed:

$$\frac{1}{k_B T_{\rm ex}} = -\frac{1}{E_u - E_l} \ln\left(\frac{N_u g_l}{N_l g_u}\right). \tag{1.3}$$

This method is most sensitive to the temperature if the expected excitation temperature is similar to $(E_u - E_l)/k_B$. Therefore, high frequency ALMA Band 9

observations, probing warm CO isotopologue lines ($J = 6 - 5$, $E_u = 111$ K) are imperative to provide a lever arm when compared with cold ALMA Band 6 ($J = 2 - 1$, $E_u = 16$ K) or ALMA Band 7 ($J = 3 - 2$, $E_u = 32$ K).

In addition, this equation is only valid if the lines are optically thin and emit from the same region and thus probe the same parcel of gas. Even though a correction for optically thick lines is mathematically possible, the molecular lines likely become optically thick at different heights in the disk, causing them to probe different layers of gas. In summary, the brightness temperature is the most suited method for optically thick emission and the line ratios is best for optically thin emission lines, see Chapter 4 for a detailed discussion.

1.5 Modelling of protoplanetary disks using DALI

Models are key to improve our understanding of protoplanetary disks as the relevant physical and chemical processes can be implemented to find trends in observables such as the morphology of the HCO^+ and N_2H^+ emission as a function of stellar type. In addition, modelling specific sources to explain the disk specific observations will give a detailed view of the temperature, density, and chemical structure in that disk. Programs that model the disk gas temperature, chemical abundances, and molecular excitation self-consistently include e.g., ProDiMo (Woitke et al. 2009; Kamp et al. 2010; Thi et al. 2011) and RAC2D (Du & Bergin 2014). The focus of this thesis is on the thermochemical code DALI (Bruderer et al. 2009, 2012; Bruderer 2013) that also includes these quantities self-consistently.

The three main sets of input parameters for a DALI model are 2D gas and dust density structure, the spectrum of the host star, and the initial chemical abundances. These are then used to calculate the abundances of the molecules included in the chemical network and raytrace the continuum and molecular line emission that can then be compared with observations of e.g., ALMA.

The first step in the DALI modelling procedure is to calculate the dust temperature using Monte Carlo radiative transfer. This 2D temperature structure, together with the radiation field, is then used as an input for the chemical network. The chemical network solver computes an initial estimate of the atomic and molecular abundances and their excitation by assuming that the gas temperature is equal to the dust temperature. Different chemical networks can be used depending on the scientific question. The smallest and thus fastest network can be used to make predictions for temperature structure and the abundance of the most abundant CO isotopologues. Other networks include isotope selective reactions for CO and H_2 (Miotello et al. 2014, 2016; Trapman et al. 2017) or additional reactions to model nitrogen bearing molecules like CN, HCN and small carbon chains as C_2H (Visser et al. 2018; Cazzoletti et al. 2018; Long et al. 2021).

In the subsequent steps, the assumption that the gas and dust temperatures are equal is relaxed as the heating and cooling rates of the atoms and molecules are used to obtain a new estimate for the gas temperature by assuming that the heating is balanced by the cooling in the disk. The new gas temperature will cause a shift in the abundances as the rate of most chemical reactions depends on the

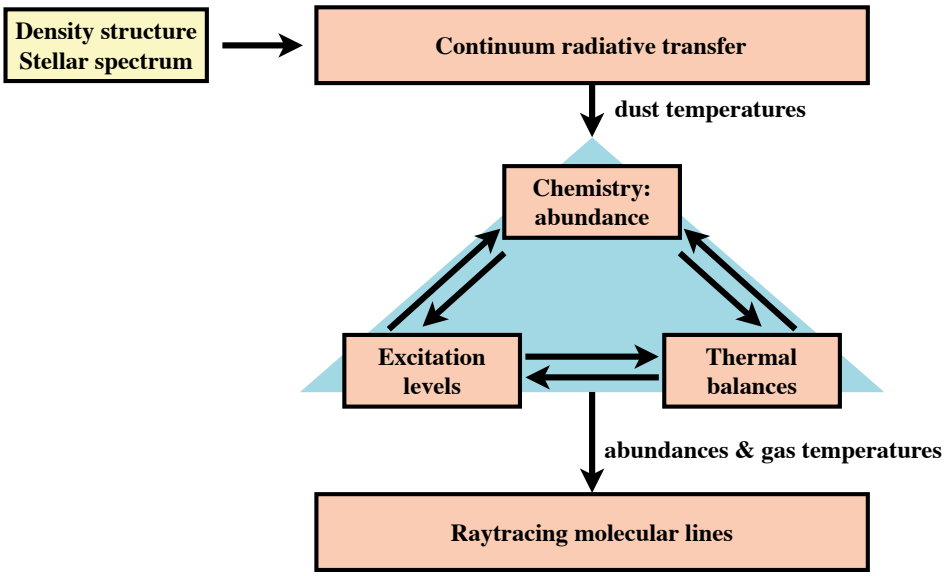

Figure 1.11: Schematic view of the work flow of DALI models (Bruderer et al. 2009, 2012; Bruderer 2013). Image credit: P. Cazzoletti, PhD thesis.

temperature. This in turn leads to new excitation levels and thus updated heating and cooling rates. Therefore, the cycle of chemistry, excitation, and thermal balance is repeated until convergence. The resulting gas and dust temperature, and abundance structure are then raytraced to create synthetic observations that can be compared to observations with ALMA or other telescopes.

The DALI modelling framework has been used to derive disk properties such as their mass an radius by comparing a population of disks observed in HD, CN, or CO isotopologues with model predictions for a set of typical disk parameters (e.g., Miotello et al. 2014, 2016; Cazzoletti et al. 2018; van Terwisga et al. 2019; Kama et al. 2020; Trapman et al. 2020). On the other hand, also in depth studies of individual disks have been used to investigate e.g., the different disk layers from the surface the the midplane, the abundance of specific atoms and molecules such as the depletion of carbon and the H_2O distribution in disks (e.g., Bruderer et al. 2012, 2014; Kama et al. 2016; van der Marel et al. 2016; Bosman et al. 2018b; Carney et al. 2018; Favre et al. 2019; Pirovano et al. 2022; Sturm et al. 2023a).

In case the modelled molecule is not included in chemical network or a specialized network is used, a parametrized abundance can be used as in input for the DALI raytracer (van der Marel et al. 2021b, see also Chapter 2). Other raytracers that can be used for this are RADMC-3D (Dullemond et al. 2012), RADLite (Pontoppidan et al. 2009), LIME (Brinch & Hogerheijde 2010), and Hyperion (Robitaille 2011).

1.6 This thesis

The aim of this thesis is to shed light on the temperature structure in protoplanetary disks, a key parameter to understand their physical and chemical structure. ALMA has revealed that structures in both the gas and the dust are ubiquitous in the brightest and largest disks. One of the biggest questions in the field is what is causing these structures. Knowledge of the gas density and thus temperature structure is crucial to discriminate between these processes. In addition, characterizing the chemical composition of both the gas and the ice is needed to understand the chemical environment in which planets are forming.

Chapter 2 investigates HCO^+ as a tracer of the water snowline in protoplanetary disks. Detailed chemical modelling using a small network dedicated to HCO^+ shows that the abundance strongly anti-correlates with that of water. Synthetic images of HCO^+ and $H^{13}CO^+$ in a typical Herbig disk show that the lack of emission in the inner disk is only for a small part due to the water snowline and primarily due to optically thick dust that hides part of the molecular line emission. In addition, the molecular excitation has a small effect on the emission. Therefore, HCO^+ and its isotopologues are most suited as tracers in disks where no optically thick dust is expected around the water snowline. One of the disks where this is the case is the V883 Ori disk around a young outbursting star. Analysing archival HCO^+ observations shows that the water snowline is located at $75-120$ au, which is much further out than the location of 40 au based on continuum observations and consistent with the radial extent of the methanol emission in this disk.

Chapter 3 further investigates the location of the water snowline in the V883 Ori disk and addresses the question if water is inherited from the earliest phases of star formation or reprocessed using the detections of HDO and $H_2^{18}O$ in this disk. The emitting surface derived from the HDO channel maps shows that this layer is very steep suggesting that the water snow surface is close to vertical. In addition, gas-phase HDO is detected out to ~ 70 au close to the disk midplane, consistent with the snowline location derived from the HCO^+ observations.

Chapter 4 focuses on the origin of the cavities seen in two transition disks, LkCa 15 and HD 169142, using both ALMA Band 6 and high frequency observations. The ratio of the warm ^{13}CO $J = 6-5$ to the cold $J = 2-1$ line shows that the LkCa15 dust cavity is warm. Additionally, no steep drop in the gas density is seen down to 10 au, resulting in a striking difference between the size of the gas cavity (10 au) and the dust cavity (68 au). Therefore, the LkCa 15 dust cavity is likely carved by multiple low-mass planets. The ^{13}CO $J = 6-5/J = 2-1$ line ratio in the HD 169142 disk results in abnormally low temperatures likely due to the vertical structure in this disk. The brightness temperature of the optically thick ^{12}CO emission shows that the gas in the dust cavity in this disk is warm at ~ 200 K and that the gas cavity is very deep with a drop of at least $200-500$ times less gas carved by a massive companion.

Chapter 5 analyses the first detection of NO in a protoplanetary disk. This disk is the major asymmetric ice trap IRS 48. A thermochemical model of this disk shows that additional NO beyond what can be produced by gas-phase chemistry is needed to explain the observations. The observed NO abundance is likely the

result of sublimating ices, indicating that the grains in protoplanetary disks carry the nitrogen and oxygen atoms that could be used in forming planets. Additionally, the non-detection of CN in this disk constrains the C/O ratio of the planet forming material to be < 1, and ≤ 0.6 in most cases.

Chapter 6 further investigates the molecular structures across the gap in a planet forming disk using thermochemical modelling. In particular, the aim of this work is to distinguish physical rings, due to a change in the density or temperature structure, from chemical rings. The models are compared to the observations of molecular rings that coincide with those seen in the dust in the HD 100546 disk (Booth et al. in prep.). The models show that only the emission of rare CO isotopologues and HCO^+ directly correlate with the amount of gas in the dust gap, whereas the column density and observed intensity of C_2H, CN, HCN, and NO stays constant or even increases for deeper gas gaps. The morphology observed in all analysed molecular tracers in the HD 100546 disk is only reproduced if the gas in the gap is depleted by at least four orders of magnitude. In addition, the effect of an increased C/O ratio, a flatter disk, and an attenuated UV radiation field are investigated. The molecular rings in the HD 100546 disk likely have a chemical origin as a deep gas gap is excluded by the observations of CO isotopologues.

This leads to the following main conclusions of this thesis:

1. HCO^+ and its isotopologues are good tracers of the water snowlines if the dust around the snowline is optically thin.

2. The 2D snow surface of HDO and methanol are very steep in the disk around the outbursting star V883 Ori.

3. The gas in the dust cavities in the HD 169142 disk and the LkCa 15 disks is warm and the cavities are likely carved by a massive companion and multiple lower mass planets, respectively.

4. The emission of gas-phase molecules seen at the location of a dust trap can give clues about the chemical composition of the ice.

In summary, molecular line observations are crucial to understand the temperature and chemical structure in protoplanetary disks. Detailed knowledge of these two parameters is key to understand the density structure and thus what is causing the rings, gaps, spirals, arcs, and young planets that are observed.

1.6.1 Outlook

ALMA has opened our view into the physical and chemical structure in protoplanetary disks over the past decade and will continue to do so in the future. Observations at high spatial and spectral resolution and sensitivity show that substructures are common in the brightest and most massive disks. One of the leading hypotheses for the cause of these structures are embedded planets but other mechanisms like snowlines, photoevaporation, and instabilities can also be responsible for the observed cavities, rings, and arcs. To distinguish these mechanisms, the gas surface density and thus the temperature needs to be measured across the

disk. Observations of many molecular lines and their subsequent analysis in six dimensions – radial, vertical, azimuthal, and the velocity in those directions – will provide crucial constraints on the origin of disk structures. The potential upgrade of the ALMA receiver bands in 2030 will double their bandwidth, allowing for simultaneous observations of multiple molecular lines (Carpenter et al. 2023).

In addition, observations of gas-phase water and water ice will provide crucial information on the chemical composition of the planet forming material. This will not only shed light on the proposed enhancement of planet formation around the water snowline, it will also provide new insights in the origin of water on Earth and its expected abundance on other forming planets. A combination of detailed studies focusing on one or a few objects together with large surveys are needed to fully understand the chemical environment in which planets are forming. Detailed studies on a single object open the opportunity to observe the weak lines that contain the most exciting information, such as the discovery of new molecules or isotopologues. Thermochemical modelling is a powerful tool to constrain the temperature, density, and chemical structure across the disks radius and height. The combination with kinematic studies characterizing the flow of gas in the disk and potentially onto planets will help to constrain which elements are accreted by young planets. In particular, the trapping of dust and their icy mantles could leave an imprint on the carbon and water abundance and thus habitability of future exo-planets. Surveys of large samples will answer some of the fundamental questions regarding the effect of spectral type and age on the chemical composition of protoplanetary disks.

While ALMA observations probe the outer disk regions, the JWST probes the hot inner disk. The warm gas lines on top of a continuum shaped by ice absorption features and silicate features provides a new window into the relevant processes in disks. The abundance of specific gas-phase molecules can not only be used to infer that the gas emits form inside the snowline of that molecule, but also to put constraints on the dust structure in this disk on scales that ALMA cannot probe (Grant et al. 2023). Additionally, the ice absorption features seen across the continuum in these sources not only reveal what ices are present but also if these ices are pristine or if ice segregation through heating has occurred (Yang et al. 2022; McClure et al. 2023; Sturm et al. 2023b). Finally, comparing JWST observations with those of *Spitzer* can provide a new window into the physical and chemical processes during outbursts (Kóspál et al. 2023), similar to what may have happend for V883 Ori. As JWST only just started observing, there are many new and exciting opportunities to come. With these new and (un)expected results, also the modelling of protoplanetary disks will need to advance to understand the newly probed disk regions.